Bacterial nanocellulose as green support of platinum nanoparticles for effective methanol oxidation

Marijana Ponjavic, Sanja Stevanovic, Jasmina Nikodinovic-Runic, Sanja Jeremic, Vladan R. Cosovic, Vesna Maksimovic

PII: S0141-8130(22)02535-1

DOI: https://doi.org/10.1016/j.ijbiomac.2022.10.278

Reference: BIOMAC 22448

To appear in: *International Journal of Biological Macromolecules*

Received date: 31 August 2022

Revised date: 26 October 2022

Accepted date: 31 October 2022

Please cite this article as: M. Ponjavic, S. Stevanovic, J. Nikodinovic-Runic, et al., Bacterial nanocellulose as green support of platinum nanoparticles for effective methanol oxidation, *International Journal of Biological Macromolecules* (2022), https://doi.org/10.1016/j.ijbiomac.2022.10.278

Bacterial nanocellulose as green support of platinum nanoparticles for effective methanol oxidation

Marijana Ponjavic[a], Sanja Stevanovic[a], Jasmina Nikodinovic-Runic[b], Sanja Jeremic[b], Vladan R. Cosovic[a], Vesna Maksimovic[c]

[a] *University of Belgrade, Institute of Chemistry, Technology and Metallurgy, Njegoseva 12, Belgrade, Serbia*

[b] *Institute of Molecular Genetics and Genetic Engineering, University of Belgrade, Vojvode Stepe 333a, Belgrade, Serbia*

[c] *Vinca Institute of Nuclear Sciences, University of Belgrade, National Institute of the Republic of Serbia, Mike Petrovića Alasa 12-14, Belgrade, Serbia*

Marijana Ponjavic, University of Belgrade, Institute of Chemistry, Technology and Metallurgy, Department of Electrochemistry, Njegoseva 12, 11000 Belgrade, Serbia
E-mail: marijana.ponjavic@ihtm.bg.ac.rs

Sanja Stevanovic, University of Belgrade, Institute of Chemistry, Technology and Metallurgy, Department of Electrochemistry, Njegoseva 12, 11000 Belgrade, Serbia
E-mail: sanjas@ihtm.bg.ac.rs (*corresponding author*)

Jasmina Nikodinovic-Runic, Institute of Molecular Genetics and Genetic Engineering, University of Belgrade, Vojvode Stepe 444a, 11000 Belgrade, Serbia
E-mail: jasmina.nikodinovic@imgge.bg.ac.rs

Sanja Jeremic, Institute of Molecular Genetics and Genetic Engineering, University of Belgrade, Vojvode Stepe 444a, 11000 Belgrade, Serbia
E-mail: sanjajeremic@imgge.bg.ac.rs

Vladan R. Cosovic, University of Belgrade, Institute of Chemistry, Technology and Metallurgy, Department for Materials and Metallurgy, Njegoseva 12, 11000 Belgrade, Serbia
E-mail: vladan.cosovic@ihtm.bg.ac.rs

Vesna Maksimovic, Vinca Institute of Nuclear Sciences, University of Belgrade, National Institute of the Republic of Serbia, Mike Petrovića Alasa 12-14, 11000 Belgrade, Serbia
E-mail: vesnam@vin.bg.ac.rs

Abstract

Bacterial nanocellulose, BNC, has emerged as a new class of nanomaterials recognized as renewable, biodegradable, biocompatible and material for versatile applications. BNC also proved as a perfect support matrix for metallic nanoparticle synthesis and appeared as suitable alternative for widely used carbon based materials. Following the idea to replace commonly used carbon based materials for platinum supports with the green and sustainable one, BNC appeared as an excellent candidate. Herein, microwave assisted synthesis has been reported for the first time for platinum nanoparticles supported on BNC as green material. Bacterial nanocelullose-platinum catalyst, Pt/BNC, was investigated by Fourier transform infrared spectroscopy (FTIR), differential scanning calorimetry (DSC), atomic force microscopy (AFM), X-ray diffractometry (XRD) and transmission-electron microscopy (TEM) analysis. The obtained results confirmed successful synthesis of new Pt-based catalyst. It was found that Pt/BNC catalyst has high electrocatalytic performance in methanol oxidation reaction. Green/sustainable catalytic system is highly desirable and provided by the elegant microwave assisted synthesis of Pt/BNC will pave the way for a larger scale application and expedite the market penetration of such fuel cells.

Keywords: bacterial nanocellulose, methanol oxidation, Pt catalyst, microwave synthesis, green support

1. Introduction

Polymer electrolyte membrane fuel cells (PEMFCs) are pure electrochemical energy converters that are key components of energy sources for vehicles and for stationary and portable energy suppliers [1]. Despite their good characteristics, such as low operating temperature, high efficiency, high energy density, and nontoxicity, PEM fuel cells are still far from large-scale commercialization since they have several unsurpassed problems. Poor durability and reliability, as well as high production costs, being the most prominent. Noble metal-based catalysts supported on the appropriate material carry the largest share of the cost in the price and durability of PEM fuel cells [2-4]. Therefore, the potential for the cost reduction is in the optimization of the catalyst, i.e. obtaining the maximum catalytic efficiency with the lowest possible content of noble metals. The majority of commercial catalysts today are Pt-based catalysts supported on porous conductive materials with a high specific surface area [3, 5, 6]. Catalysts support has significant impact on nanostructured noble metal catalyst's activity and stability because interaction between the metal particle and the support can affect metal particle size and dispersion [7]. The function of the support is also to extend the surface area of the metal that is, to enable efficient utilization of metals by providing the maximum ratio of surface area and weight. Due to their large surface area and excellent conductivity and stability, over the last few decades, commonly used catalysts supports have been carbon based materials such as Vulcan XC-72 carbon black (CB), multi-walled carbon nanotubes (MWCNTs) and graphene [8-11]. However, their production process includes pyrolysis of coal or petroleum releasing carbon dioxide and other harmful organic products into the atmosphere and having a negative influence on the environment.

Since the focus of upcoming science and technology is rapidly shifting towards environmentally friendly, sustainable and renewable resources, cellulose as a "green" material appeared as perfect candidate for metal nanoparticles support [12]. Cellulose is the most available biomacromolecule in nature that can be obtained from various sources such as wood, cotton, crops, cellulosic agricultural wastes, and more recently from bacterial fermentations (*Komagataeibacter medellinensis*, *Gluconacetobacter xylinus*) [13-15]. It is renewable, biodegradable and biocompatible material that can be easily converted into derivatives producing a new class of nanomaterials suitable for various applications: food packaging, biomedical, pharmaceutical, water treatment, energy, electronics, biosensors, etc. [16, 17]. Bacterial

nanocellulose, BNC, has gain on its popularity due to its outstanding performances such as high crystallinity, high aspect ratio, surface reactivity, low density, low cytotoxicity, availability, appropriate porosity, high water retention capacity, superb overall mechanical properties [18-21]. BNC is also promising material for production of cellulose nanocrystals, CNs, by controlled hydrolysis under different conditions [22, 23], which was further recognized in the applications of enzyme immobilization [24], drug delivery [25] and green support for metallic particles fabrication [26]. Remarkable research interest has been focused on oxidation of BNC [27, 28] in order to produce improved material with great potential in tissue engineering [29, 30], as high-performance separators in lithium-ion batteries [31], but also as metal support nanoparticles with superior catalytic properties [32]. BNC has already been recognized as solid support of palladium and copper nanoparticles in the transition metal catalyzed cross-coupling reactions [26].

While many reports have demonstrated that metallic nanoparticles such as gold, silver, copper and palladium supported on bacterial nanocellulose can be successfully used for various catalytic performances [12, 33-36], studies referring to platinum based catalysts with BNC as metallic carrier have been very limited [37]. Further, electrocatalytic performance for direct methanol fuel cells (DMFC) of carbonized bacterial cellulose-Pt composite has been investigated by Huang et al. [38]. Direct methanol fuel cells have been intensively assessed as very promising power sources due to environmental and economic advantages of methanol as a fuel. Methanol is a clean-burning, biodegradable fuel that can be made from a wide array of feedstocks. As a fuel in fuel cells technology, it comes with a high energy density (6 kW/kg), efficient combustion, ease of distribution and wide availability around the globe [39, 40].

Given that the potential of BNC in energy storage has been proved [41], the additional application of BNC in the area of electrochemistry was investigated for energy conversion purpose. The major goal of this study was to use and validate BNC as metallic nanoparticles support instead of carbon based platinum supports using microwave assisted, synthetic procedure for Pt carbon catalyst preparation. Herein, quite fast and very effective microwave assisted method to synthesize Pt nanoparticles deposited on bacterial nanocellulose, Pt/BNC, obtained by *K. medellinensis* has been reported for the first time. The catalytic activity was evaluated using the methanol oxidation reaction whereby Pt-bacterial nanocellulose supported catalyst indicated remarkable catalytic performance. By applying new approach, microwave reduction of platinum,

sustainability and environmentally friendly aspects of BNC were emphasized, which along with possibility of low-cost production of BNC in large quantities makes Pt/BNC catalyst suitable for scale-up.

2. Experimental

2.1. Bacterial nanocellulose production

Bacterial nanocellulose (BNC) was produced using *Komagataeibacter medellinensis* ID13488 strain (CECT 8140 (Spanish Type Culture collection)). Strain was cultivated in a standard Hestrin–Schramm medium (HS) containing 20 g/l glucose, 5 g/l peptone, 5 g/l yeast extract, 2.5 g/L Na_2HPO_4 and 1.15 g/l citric acid, at pH 4.5 under static conditions for 7 days, and BNC discs with an 10 cm diameter were obtained from bacterial growth. Under these conditions, 6 g/l of BNC was produced. Discs were treated with KOH (1 M), extensively washed with deionized H_2O until a pH of 7.0 was reached and were then dried under warm air at 45 °C for 6–8 h.

2.2. Catalyst preparation

Synthesis of the Pt nanoparticles supported on bacterial nanocelullose was obtained using the microwave-assisted polyol method. In this procedure, 1 ml of 0.05 M hexachloroplatinic acid, H_2PtCl_6, were mixed with 20 ml of ethylene glycol in a 100 ml beaker under magnetic stirring. Then, 0.8 M NaOH was added dropwise to adjust pH~12. The prepared solution was placed in the center of the microwave oven and the reduction reaction was performed by microwave irradiation at 700 W during 60 s. After microwave heating, the colloidal solution was mixed with 150 ml 2 M H_2SO_4 and BNC suspension (20 mg of BNC was suspended in 10 ml of distilled water and fibrillated by ultrasonic homogenizer in three cycles for 3 min, under the frequency of 20 kHz), and left under magnetic stirring for 3 h in order to obtain the uniform deposition of the colloids on the BNC substrate. The resulting suspension was filtered using a vacuum pump, washed and the solid residue was washed thoroughly with high purity water (Millipore, 18 MΩ cm) until neutral pH value was reached. The solid product (in the form of film), Pt/BNC, was dried in an oven at 40 °C till the constant mass was achieved. Nominal Pt loading for prepared catalysts was adjusted to ~ 30 mass % calculated to the catalyst mass (9.8 mg of Pt estimated from the 1 ml of 0.05 M hexachloroplatinic acid added to the reaction mixture). The yield (%) of the obtained catalyst was calculated according to equation (1):

$$\text{Yield (\%)} = m_{exp}/m_{theor} \text{ x } 100 \text{ \%} \quad (1),$$

where m_{exp} is physical mass of obtained dry, solid Pt/BNC catalyst in the form of film, while m_{theor} is theoretical value of catalyst including mass of Pt (9.8 mg) and BNC mass in feed (20.0 mg).

2.2.1. Synthesis of modified BNC, *m*-BNC

For the comparison purpose and for the estimation of Pt amount in Pt/BNC catalyst by thermogravimetric analysis, modified BNC, *m*-BNC, was also synthesized. The identical synthetic procedure applied for the synthesis of Pt/BNC was used, but the step of addition of Pt colloid was omitted. Hence, 20.0 mg of dry BNC was suspended in 10 ml of deionized water, treated by ultrasonic homogenizer in three cycles for three minutes, under the frequency of 20 kHz, then 150 ml of 2 M H_2SO_4 was added and the reaction mixture was left for three hours under vigorous stirring. The reaction mixture was filtrated, washed with deionized water and dry at 40 ^oC till constant mass. The yield of obtained *m*-BNC was high, 94 %.

2.3. Preparation of the electrodes

Glassy carbon (GC) disc (Sigradur-Sigri, Elektrographite, GMbH, Germany), 5 mm in diameter was used as a working electrode. Mechanical treatment of glassy carbon surfaces before each experiment has consisted of abrasion with silicon carbide papers of decreasing grain size, followed by polishing with alumina of 1-, 0.3- and 0.05-μm particle size, and finally washing with ultra-pure water. Water suspensions of synthesized catalysts with the addition of Nafion solution ((2 mg catalyst powder + 50 μl Nafion)/1 ml ultra-pure water, prepared in an ultrasonic bath) were drop cast onto the freshly polished GC surfaces (10 μl) and dried at room temperature.

2.4. Characterizations

2.4.1. ATR- Fourier Transform Infrared Spectroscopy (ATR-FTIR)

The Fourier transform infrared spectroscopy was used to confirm the structure of bacterial nanocellulose before and after synthesis of Pt/BNC catalyst in microwave. All samples were subjected to IR-Affinity spectrophotometer (Thermo Scientific, NICOLET iS10) in an attenuated total reflection (ATR) mode with a resolution of 4 cm^{-1} with the predefined range of 4000 to 400 cm^{-1} at room temperature. The number of scans was fixed to 32.

The recorded FTIR spectra were used to calculate the degree of oxidation (DO) of BNC according to the following equation (2) [27] :

$$DO = 0.01+0.7 \text{ x } (I_{1630\text{-}1640} / I_{1029}) \quad (2),$$

where $I_{1630\text{-}1640}$ and I_{1029} correspond to the intensity of carboxyl group and the highest absorbance peak (attributed to the C-O-C stretching vibrations), respectively.

2.4.2. Differential scanning calorimetry and thermogravimetric analysis (DSC/TG)

Coupled differential scanning calorimetry (DSC) / thermogravimetric (TG) analysis was performed on a TA Instruments SDT Q600. The BNC and Pt/BNC samples were measured in a temperature range of 25 °C to 900 °C, at the heating rate of 10 °C/min, in a nitrogen atmosphere. Melting temperature, T_m, and melting enthalpy, ΔH_m, obtained from DSC analysis were calculated by TA Universal Analysis software. Weight of samples was about 3 mg. The Pt yield supported at BNC was estimated from the weight remained at temperature of 800 °C.

2.4.3. Wide angle X-Ray diffraction analysis (XRD)

The phase analysis of raw BNC and Pt/BNC catalyst was conducted by using X-ray diffractometer (XRD) Rigaku Ultima IV, Japan, with CuKα1 radiation (λ = 0.154178 nm). The X-ray diffraction data were collected over the 2θ range from 5° up to 90° with the step of 0.02° and scanning rate of 5°/min. The PDXL2 2.0.3.0 software with reference to the diffraction patterns available in the International Center for Diffraction Data (ICDD) was used for the phase identification and data analysis.

2.4.4. X-Ray Photoelectron Spectroscopy analysis (XPS)

Surface composition of Pt/BNC catalyst was investigated by XPS using SPECS Systems with XP50M X-ray source for Focus 500 and PHOIBOS 100/150 analyzer employing AlKα source (hv = 1486.74 eV) at a 12.5 kV and 32 mA. The XPS spectrum (1000–0 eV binding energy) was recorded at constant pass energy of 40 eV, step size 0.5 eV and dwell time of 0.2 s in the FAT mode. Spectra of C 1s, O 1s, and Pt 4f peaks were obtained using constant pass energy of 20 eV, step size of 0.1 eV and dwell time of 2s in the FAT mode. Pressure in the chamber was set to 9 x 10^{-9} mbar during the measurements. All peak positions were corrected with respect to the C 1s peak at 284.8 eV. Spectra were analyzed with commercial CasaXPS software.

2.4.5. Transmission electron microscopy analysis (TEM)

Transmission electron microscope (TEM) JEM-1400 with an accelerating voltage of 120 kV during the measurements was used for detailed characterization of the microstructure of BNC and Pt/BNC materials. The samples were prepared by ultrasonically treated water suspension of BNC and Pt/BNC and applying a drop of the suspension onto the carbon-coated copper grid. Images captured at different magnifications were processed by ImageJ software to estimate the

average diameter and Pt nanoparticles size distribution. For that purpose, more than 200 separate particles were measured.

2.4.6. Atomic Force Microscopy analysis (AFM)

The surface morphology was investigated by atomic force microscopy (AFM) with NanoScope 3D (Veeco, USA) microscope operated in tapping mode under ambient conditions. Silicon probe with spring constant 40 Nm^{-1} was used. Image analysis was done by Nanoscope image processing software. Water suspensions of bacterial nanocellulose and Pt/BNC catalyst were deposited on a polished mica substrate and air-dried for 30 min.

2.5. Electrochemical measurements

All of the electrochemical experiments were performed at room temperature in a three-electrode-compartment electrochemical cell with a Pt wire as the counter electrode and a bridged saturated calomel electrode (SCE) as reference one.

The electrocatalytic activity of all catalysts was studied in 0.5 M H_2SO_4 + 0.5 M CH_3OH solution. Methanol was added to the supporting electrolyte solution while holding the electrode potential at – 0.2 V. The reaction was studied at *as-prepared* Pt/BNC surfaces (surfaces without any previous treatment in the basic electrolyte).

Long-term catalyst stability was investigated for methanol oxidation reaction during 100 cycles in potential range from -0.25 V to 0.9 V and by chronoamperometric measurement. Current-time transient curve was recorded after immersion of freshly prepared catalysts in 0.5 M H_2SO_4 + 0.5 M CH_3OH solution and holding electrode at 0.2 V vs SCE for 30 min.

The electrochemical surface area (ECSA) of Pt/BNC catalyst surfaces was calculated assuming that during hydrogen adsorption on platinum monolayer formation of hydrogen happens and the total charge corresponding to monolayer was $Q_{tot.}$= 210 μC/cm^2 [42]

All solutions were prepared from Merck p.a. reagents with high purity water. The electrolytes were purged with purified nitrogen prior to each experiment. AUTOLAB potentiostat/galvanostat PGStat 128N (ECO Chemie, The Netherlands) was used in electrochemical experiments.

3. Results and discussion

Recognized as a green platinum support with the great potential in the electrochemistry oxidation, BNC was successfully applied for the microwave assisted synthesis of Pt-based catalyst in a new synthetic route (Figure 1). For that purpose, microwave reduction of Pt(II) to

Pt(0) using ethylene glycol as both reducing and stabilizing agent was performed followed by the treatment of sulfuric acid producing Pt supported BNC film suitable for the methanol oxidation. Ultrasonication step was also performed to allow increased homogeneity of the material. The yield of the synthesized Pt/BNC catalyst was quite high, 92 %, confirming successful synthesis and efficiency of applied reaction conditions.

3.1. FTIR analysis

Fourier transform infrared spectroscopy (FTIR) is a useful tool to get rapid information about the changes in structure of BNC after catalyst's synthesis. The FTIR spectrum of BNC used for the synthesis (raw BNC) indicated typical characteristic peaks of cellulose as shown in Figure 2. The broad peak located in the area of 3000 to 3500 cm^{-1} in both raw BNC and Pt/BNC is assigned to –OH stretching vibrations, while the –C-H stretching vibrations at 2850-3000 cm^{-1} and C-O and –C-O-C stretching of glycoside bond in the area of 970-1160 cm^{-1} in cellulose can be also seen clearly [32]. In the FTIR spectrum, vibration band at 1427 cm^{-1} (attributed to the O-C-H and H-C-H deformation) but also –C-H vibration bands at 1320 cm^{-1} and 890 cm^{-1} were confirmed as well [27]. The peak at wavenumber of 1640 cm^{-1} in the spectrum of raw BNC corresponds to the carboxylic groups in the ionized form $-COO^-Na^+$ provided by the neutralization of BNC suspension with sodium hydroxide, NaOH [43, 44]. Sulfuric acid used in the synthesis procedure provided better support for Pt nanoparticles on the BNC surface through the introduction of HSO_3^- groups. Comparing the spectra of raw BNC and Pt/BNC catalyst, a new, small intensity peak located at 1710 cm^{-1} was detected, corresponding to the carbonyl –C=O group stretching indicating the oxidation of BNC after Pt/BNC synthesis[12] as a consequence of hydrothermal reaction upon treatment with 2 M H_2SO_4. Characteristic peaks coming from the –C-O and –C-O-C stretching remained unchanged after synthesis (highlighted area in the FTIR spectrum) suggesting that the ring structure of BNC was not changed and the secondary hydroxyl groups on the ring structure remained while the oxidation mostly occurred at the primary hydroxyl groups due to the higher reactivity [12]. When the BNC suspension was added in the solution containing previously reduced Pt (0) from Pt (II) thought the microwave treatment, the electron reach, oxygen containing groups ($-COO^-$ and -OH) behave as an anchor point to immobilize Pt nanoparticles by the complexion or through the electrostatic interactions [45]. Shifting of the $-COO^-$ characteristic peak from 1643 cm^{-1} to 1628 cm^{-1} suggested the existence of the interactions between Pt nanoparticles and abundant functional groups on the BNC surface.

Additionally, the degree of oxidation (*DO*) (Table 1) implied the significant increase from 0.14 (calculated for raw BNC) to 0.40 for Pt/BNC defining the total amount of carboxyl groups introduced after the microwave synthesis of Pt supported catalyst using sulfuric acid.

3.2. DSC analysis

The DSC analysis depicted three distinct regions of thermal profiles with two endothermic peaks in the case of raw BNC, while in the case of synthesized Pt/BNC catalyst, additional exothermic peak was detected (Figure 3a). The first exothermic peak at 114.2 °C in the DSC thermogram of Pt-BNC corresponded to the heat of vaporization of adsorbed moisture. The second endothermic peak for all samples at higher temperatures appeared as crystalline melting temperature, T_m, of BNC (Table 1). Those values of the raw BNC and Pt/BNC was very similar, about 200 °C, but with the remarkable difference in the melting enthalpies, ΔH_m, which was calculated to be 50.9 J/g for the Pt/BNC in comparison to extremely small ΔH_m of 9.3 J/g measured for the raw BNC. The second endothermic peak was detected at higher temperature region, between 300 and 350 °C that corresponded to the degradation of cellulosic material, T_d. In the case of catalyst Pt/BNC, this peak was clearly visible at temperature, T_d, of approximately 341 °C, with the enthalpy of ΔH_d = 210.3 J/g. All aforementioned results are in correlation with previous results found in various studies [22, 46, 47].

Table 1. Results of degree of oxidation, *DO*, and DSC/TG analysis (melting temperature, T_m, melting enthalpy, ΔH_m, maximum degradation temperature, T_{max})

Sample	*DO*[a]	T_m, °C[b]	ΔH_m, J/g[b]	T_{max}, °C[c]	Residual weight at 800 °C, %[c]
BNC	0.14	200.7	9.3	340/616	20.4
Pt/BNC	0.40	200.5	50.9	328/603	56.8

[a] according to FTIR analysis, [b] according to DCS analysis, [c] according to TG analysis

3.3. TG/DTG analysis

Thermal stability of investigated BNC based materials and Pt/BNC catalyst was presented in Figure 3b. The first stage of weight loss, occurring approximately at 50 – 120 °C, was mainly due to evaporation of residual moisture, existing in either free or bound water [14]. The main thermal degradation stage, at which the highest weight loss was detected, happened at the

temperature range of 220 – 340 °C, when most of the cellulosic material was degraded. The maximum degradation temperature, T_{max}, at this stage, for raw BNC was 340 °C, while the Pt/BNC catalyst showed T_{max} at 328 °C (Table 1). The lower thermal stability of Pt/BNC was not surprising since the treatment with sulfuric acid during the synthesis disrupted the BNC structure, and the increased surface area with smaller particle size probably increased heat transfer rate [48]. Despite the most of cellulosic material degraded over the temperature of 400 °C, the third thermal event, extended from 450 to 620 °C, converting cellulose to gaseous products and CO_2 [22]. Residual mass of raw BNC at 800 °C was 20.4 %, while from the residual mass of the Pt/BNC it was possible to estimate the amount of absorbed platinum. In order to estimate the amount of Pt with the most precision, modified BNC, *m*-BNC, was synthesized, when identical reaction conditions were applied without the addition of platinum. Modified BNC had a residual mass of 26.5 %, and Pt/BNC had 56.8 % of residual mass at 800 °C. According to TGA results, 30 mas% of Pt was absorbed on BNC as support, which perfectly meet the targeted value of 32 %, confirming the successful microwave assisted synthesis of Pt/BNC catalyst. Thermal degradation profile of *m*-BNC differed greatly in comparison to raw BNC and Pt/BNC, with the decreased thermal stability (T_{max} at 227 °C followed by the small degradation peak at 374 °C) which is probably due to the introduction of carboxylic groups on the surface, similar like with the TEMPO oxidized BNC [49]. Although the same procedure was applied for the synthesis of Pt/BNC catalyst, Pt/BNC indicated better thermal stability in comparison to *m*-BNC, which could be explained by the interactions between Pt and BNC proved by FTIR analysis.

The thermogravimetric analysis provided information on the carbon content of the samples. Carbonization efficiency, *CE* (%), of raw BNC and *m*-BNC (modified by 2M H_2SO_4, equal to BNC in Pt/BNC catalyst), could be calculated from weight loss at different annealing temperatures [50]. At the starting annealing temperatures up to 350 ^oC, reduce in weight occurs due to the loss of water and moisture in material, while sharp weight loss, when the most of the mass was reduced, occurs at temperature interval of 350 ^oC to 600 ^oC which was ascribed to the combustion of residual carbon (depolymerisation of cellulose) [51]. The results presented in Figure S1 demonstrated that the carbon content after 350 ^oC of *m*-BNC was higher, *CE* of 42 %, in comparison to raw BNC, *CE* of 32 %, and this trend could be observed up to 800 ^oC (when *CE*

of BNC was 21 % and *CE* of *m*-BNC was 31 %) confirming the higher carbonization efficiency of the modified BNC.

3.4. XRD analysis

The XRD diffraction patterns of the native, raw BNC and catalyst Pt/BNC are presented in Figure 4. In the recorded diffractogram of raw BNC, four diffraction peaks were detected. Three 2θ diffraction peaks at 14.7°, 16.9° and 22.9° are attributed to the crystallographic planes ($1\,\bar{1}\,0$), (110) and (200), respectively, and these three characteristic peaks are prevalent in cellulose with triclinic crystal lattice [22] [52]. Peak at 2θ = 34.3° corresponds to the plane (004) verifying monoclinic crystal structure of cellulose. The type of the crystal lattice depends on the nanocellulose sources and the obtained results are in agreement with previous studies [53].

In the XRD crystal patterns of Pt/BNC catalyst, BNC characteristic diffractions peaks of the highest intensity (2θ around 14.7° and 22.9°) were preserved, while other peaks were characteristic diffraction peaks of *fcc* platinum crystal structure at 40.5° (111 plane), 46.6° (200 plane), 67.8° (220 plane) and at 81.6° (311 plane) [54, 55]. Furthermore, no shifting of the detected BNC diffraction peaks position in Pt/BNC diffractogram was detected indicating that the dimension of crystal lattice staved unaltered. In addition, by applying PDXL2 2.0.3.0 software, it was possible to estimate the Pt crystallite size in the synthesized Pt/BNC which was about 1.8 nm. Pt crystallite size depends on various parameters such as type of support, preparation method, reaction conditions, presence of other metals, amount of reducing and stabilizing agents, etc.), and the calculated value of 1.8 nm is close to those obtained for Pt/C catalyst (2.9 nm) [56] while it is remarkably lower to those obtained by *B.Ruiz-Camacho et al.* [57] who find the crystallite size of 10.1 nm for Pt/C and 8.1 nm for Pt supported on carbon nanotubes. The amount of capping agent in synthesis notably defines the crystallite size, and for the Pt/C catalyst it varies from 2 nm to 6 nm depends on amount of used capping agent [55].

3.5. XPS analysis

In order to evaluate the chemical state of platinum nanoparticles, synthesized Pt/BNC catalyst was submitted to X-ray photoelectron spectroscopy analysis. Recently, this technique has been very popular for the surface identification of polymers, but its main disadvantage is that it identifies only few nanometers and assumes the identity of the bulk. Moreover, in the case of

organic materials, like BNC, sample deterioration due to high vacuum and exposure to X-ray could happen, while charging might induce significant changes in carbon and oxygen peak shapes [58]. However, XPS provides an important information of surface composition and oxidation state of metals, and further indicate the success of metallic nanoparticles deposition on BNC surface as solid support. The XPS spectra of Pt/BNC catalyst is presented in Figure 5. In the survey spectrum of the sample (Figure 5a), presence of carbon (C 1s), oxygen (O 1s, O 2s) and platinum (Pt 4f) was confirmed. By using CasaXPS software, C 1s peak was deconvoluted into three curves (Figure 5b), where peak at 284.4 eV is attributed to C-C bond from glucopyranose ring, while peak at 284.9 eV corresponds to single –C-O- bond. At the highest binding energy, 285.8 eV, green peak is ascribed to -C=O [59]. The highest binding energy peak of O 1s was also analyzed by dividing into three peaks at 530.7 eV, 531.1 eV and 532.0 eV (shown in Figure 5c) that could correspond to -C=O, C-O and –O-H bands, respectively [51]. The Pt-BNC catalyst shows two main peaks at binding energy values of 74.4 eV and 71.1 eV which could be assigned to Pt^0 $4f_{5/2}$ and Pt^0 $4f_{7/2}$, respectively. The deconvolution of platinum 4f spectrum suggested that Pt^{2+} and Pt^{4+} species were converted into Pt^0 over microwave reduction. The content of metallic Pt^0 in support depends on various parameters: reduction method (pyrolysis, reduction chemical agents, microwave), interaction between metallic particles and support, particles size [60-62]. Absence of other peaks except those related to metallic Pt provide the evidence of efficient microwave assisted reduction.

3.6. AFM analysis

Dimensions and geometry of BNC materials and Pt/BNC catalyst were examined by the AFM technique and are shown in Figure 6a. BNC forms a film with a nanofibers structure where nanofibers have a high aspect ratio and thus a highly developed surface. As a result of the interaction between the nanocellulose particles, the nanofibers form a network. In addition, it was experimentally found that the diameter of separate nanocellulose fibers ranges from 100 nm to 140 nm, and their length is ~ 1μm. The diameter of separate nanofibers is within the range of 40 nm. AFM image of Pt deposited on BNC reveals a structure composed of spherical shaped agglomerates with a pretty uniform size of ~ 300 nm. After the deposition of Pt particles on BNC support, diameter of separate BNC nanofibers remained unchanged.

3.7. TEM analysis

The microstructure of raw BNC and catalyst Pt/BNC was investigated by TEM analysis and the captured bright-field images are presented in Figure 6b. The raw BNC indicated very porous 3-dimensional structure. Microstructure of the BNC in the catalyst Pt/BNC was different in comparison to raw BNC, since the BNC passed through the mechanical disintegration and chemical treatment (hydrothermal reaction) over the synthetic procedure. Therefore, fine, smooth BNC structure was disintegrated into small fragments that formed compact, plane structure with clearly visible Pt particles supported on its surface (appeared as small, black dots). The obtained less fibrous BNC structure in catalyst is due to the both delamination process which diminished the interlayer hydrogen bonding between the cellulose polymer chains (hydrogen bonding was also interrupted after treatment of H_2SO_4), but also due to the formation of BNC gel well dispersed in aqueous solution used for the TEM samples preparation. Despite few visible aggregates of Pt particles, more separate, well dispersed Pt particles were also captured with quite uniform distribution and the dominant particles sizes of (3.4 ± 1.04) nm (histogram of particle size distribution showed in Figure 6b).

3.8. Electrochemical performance of the catalysts

The electrochemical behavior of Pt/BNC catalyst was determined by cyclic voltammetry measurements. The basic cyclic voltammogram of Pt/BNC catalyst is illustrated in Figure 7a. Figure 7a shows the cyclic voltammograms curves (CV) for the *as-prepared* Pt/BNC catalyst. The voltammogram is similar to the voltammograms that can be found in the literature for platinum catalysts synthesized in the same way on high area carbon surfaces [63, 64]. The potential region from -0.25 V to 0.1 V presents hydrogen adsorption/desorption region. As can be seen from the hydrogen region, characteristic peaks that should denote (110) and (100) sites of polycrystalline Pt particles [65] are not clearly discernible. This can be explained by the fact that Pt/BNC catalyst are applied on GC surface from water suspension and dried in the air, so different oxygen and/or carbon-containing species are probably adsorbed at catalysts surface containing low coordinated Pt atoms. Vaguely defined peaks are a consequence of displaying the first cyclic voltammogram of Pt/BNC.

The shapes of the CV for BNC is typical for nanocelulose materials and in the potential region between the oxygen evolution and hydrogen adsorption shows that no reactions occurred, other

than electrostatic charging and discharging. CV for Pt/BNC catalyst obtained in the first cycle (*as-prepared* Pt/BNC electrode) and CV recorded after electrochemical treatment comprising 30 cycles in the supporting electrolyte (oxide-annealed Pt/BNC electrode) were presented in Supplementary file (Figure S2).

3.9. Methanol oxidation

The methanol oxidation reaction can take place in one of two reaction ways illustrated in the Scheme 1:

$$CH_3OH \rightarrow \text{adsorbed intermediates} \rightarrow CO_{ads}$$
$$\downarrow \qquad\qquad \downarrow$$
$$HCHO, HCOOH \rightarrow CO_2$$

Scheme 1. Methanol oxidation reaction pathways.

The ideal methanol oxidation reaction in DMFCs would be direct oxidation of methanol to CO_2 and transfer of six electrons. However, the overall reaction for methanol oxidation occurs in the few steps with main processes being the adsorption of methanol and its dehydrogenation, followed by adsorption of carbon-containing intermediates such are CO_{ads} , water dehydrogenation, formation of OH_{ads} which are necessary for CO_{ads} oxidation and finally production of CO_2 [66-68]. The intermediate product CO_{ads} is always present in the real process, it blocks the catalysts surface covers the active sites and decrease catalyst performance. Oxidation of CO_{ads} starts when oxygen-containing species obtained in the interaction of water with platinum are produced in a sufficiently large quantity to giving CO_2 in the Langmuir-Hinshelwood type of reaction (equation 3) [55, 69, 70]:

$$CO_{ads} + OH_{ads} \rightarrow CO_2 + H^+ + e^-. \qquad (3)$$

Thus, effective removal of CO_{ads} will have a great influence on the methanol oxidation activity.

The activity of the Pt/BNC catalyst for methanol oxidation was evaluated from potentiodynamic measurements (Figure 7b).

Figure 7b shows that the methanol oxidation reaction starts in the region where the hydroxyl ion adsorption occurs (0.15V), which are also quite low potential values and indicate good catalyst activity. The Pt/BNC catalyst has negative shifts of the onset and peak potentials in comparison to Pt/C-E-TEK commercial catalyst which indicate that Pt/BNC catalyst is able to significantly reduce the over-potential for methanol oxidation. These improvements can be attributed to the

presence of oxygen containing functional groups on the BNC surface, actually to the effective functionalization of BNC support over synthesis process. It is well known that –OH groups are active intermediates in the methanol oxidation [71]. Applied synthesis procedure provided the increase of acidic functional groups ($-COO^-$) on the support improving the interactions of Pt particles and BNC and also increasing the fraction of oxygen-containing species (-OH) on Pt/BNC catalyst [7]. Further, most of the studies imply that optimal Pt particles' size required for the effective catalyst activity is below 4 nm. According to TEM analysis results, Pt particles' size of the obtained Pt/BNC catalyst were ~ 3.4 nm (Figure 6) additionally contributing to the high catalytic activity in methanol oxidation reaction. The potential maximum is on ~ 0.55 V which is in accordance with literature data for the methanol oxidation on platinum catalysts supported on high area carbon materials [69, 70].

The peak current densities for methanol oxidation reaction are 0.82 mA/cm^2; 0.48 mA/cm^2; 1.48 mA/cm^2; for Pt/BNC, Pt/C and Pt/C E-TEK catalyst, respectively.

Electrocatalytic stability of the Pt/BNC catalyst was examined by prolonged cycling (100 cycles) as well as by chronoamperometric measurements in H_2SO_4/CH_3OH solution. Lowering of initial activity after 100 cycles in methanol oxidation reaction is shown in Figure 7c. It can also be observed that the peak current in the forward (anodic) scan is higher than in the reverse (cathodic) scan for both the initial and the 100th cycle. It is well known that the peak current in reverse scan is related to the removal of the incomplete oxidized carbonaceous species, such as CO, $HCOO^-$ and HCO^-, accumulated on the catalyst surface during the forward anodic scan. CO is a crucial unwanted intermediate of methanol oxidation which can poison Pt catalyst for the methanol oxidation. As a result, the ratio between the forward and reverse scan peak currents (j_f/j_b) can be used to define the tolerance of the catalyst to CO [70, 72, 73].

A low j_f/j_b value usually indicates poor oxidation of methanol to CO_2 during the forward anodic scan and excessive accumulation of residual carbon species on the catalyst surface. On the other hand, a higher j_f/j_b ratio is indicative of improved CO tolerance. Actually, a higher ratio corresponds to a lower j_b peak, which suggests that less unwanted CO molecules are adsorbed on the catalyst surfaces.

As the number of cycles increases, participation of direct path in methanol oxidation reaction decreases, while the role of indirect path increases. In our study, Pt/BNC catalyst shows slightly better j_f/j_b value (j_f/j_b = 1.62) than Pt/C catalyst synthetized by the same method but with Carbon

Vulcan XC as a support (j_f/j_b = 1.45). In comparison to commercial Pt/C E-TEK (j_f/j_b = 0.99) Pt/BNC catalyst has better j_f/j_b value since mass loading of Pt in Pt/C E-TEK catalyst is significantly higher than in Pt/BNC catalyst [74]. Moreover, Pt/NC catalyst synthetized using similar microwave-assisted polyol method in ethylene glycol solution from green biomass chitosan and carbon black as a support appears to have lower values of both j_f/j_b (0.98) and j_f max (0.38 mA/cm^2) in comparison to Pt/BNC [75]. The electrochemical performances comparison with Pt catalyst supported on N-doped carbon nanofibrous networks (prepared by ecofriendly precursors, bacterial cellulose and urea), Pt/NBC-1000, indicated slightly lower values of j_f/j_b but higher j_f max compared to synthesized Pt/BNC [76].

This suggests that the Pt/BNC catalyst is capable of efficiently oxidizing methanol molecules, i.e. generating less poisoning species, thus providing better CO tolerance. All values for j_f/j_b ratio are summarized in Table 2.

Table 2. Peak currents ratio between the forward and backward scan (j_f/j_b) obtained for Pt/BNC, Pt/C, Pt/C Tanaka, Pt/NC and Pt/NBC-1000 catalysts.

Catalyst	Pt/BNC	Pt/C [70]	Pt/C E-TEK [74]	Pt/NC [75]	Pt/NBC-1000 [76]
	(30 %wt Pt)	(25 %wt Pt)	(47 %wt Pt)	(20 wt% Pt)	(18 wt% Pt)
j_f/j_b	1.62	1.45	0.99	~ 0.98	1.06
j_f max (mA/cm^2)	0.82	0.48	1.48	0.38	0.94

It should be also noticed that the initial part of the anodic curve for the first cycle of the Pt/BNC catalyst appears a slight indication of the voltammetric characteristic of the hydrogen desorption region. Its presence indicates that the surface of the catalyst is not blocked by products of dissociative adsorption of methanol, during the application of a potential of -0.2 V on the working electrode for 3 min before the start of cyclization of the electrode in the potential range from -0.2 V to 0.9 V.

Testing of the tolerance of the synthesized catalyst to catalyst deactivation during the methanol oxidation by chronoamperometric measurement, shows a good agreement with the potentiodynamic tests (Figure 7). The current drops sharply at the beginning of the experiment, and then the current decreases very slightly during the duration of the experiment. The decrease in activity is related to accumulation of unwonted intermediate species, especially of the

adsorbing CO species on the Pt/BNC surface. Both stability test reactions are in a very good agreement with our previously published results in which the Pt/C catalyst is synthetized by microwave assisted method on the Carbon XC Vulcan support. The obtained results for Pt/BNC catalyst again prove the lower poisoning, indicating better stability and higher tolerance to CO-like intermediates.

4. Conclusions

Platinum nanoparticles deposited on BNC as a green supporting material were successfully synthesized by the microwave irradiation method, which was the first time that microwave assisted synthetic procedure was applied for Pt/BNC system. FTIR analysis confirmed the interactions between Pt nanoparticles and functional groups on BNC surface, but also the additional functionalization of BNC through the synthesis of catalyst due to the sulfuric acid treatment. The amount of Pt adsorbed on BNC surface was calculated to be ~ 30 mas%, according to TG/DTG analysis, coupled with almost quantitative yield indicated successful synthesis of Pt/BNC catalyst and the significance of the synthetic procedure. Successful deposition of Pt nanoparticles was additionally proved by XRD analysis. Further, XPS and TEM analysis confirmed the presence of peaks related to metallic Pt and that Pt nanoparticles were well dispersed onto BNC surface with the particles size of 3.4 mm. Importantly, Pt/BNC catalyst was validated for the potential application in the fuel cells for methanol electro-oxidation reaction. Successful methanol oxidation, high catalytic activity, negative shift of the onset potential, stability, great tolerance to CO species, of Pt/BNC catalyst suggest BNC as suitable alternative for carbon based materials as Pt support. The observed great catalytic activity in methanol oxidation, comparable with those obtained for Pt-carbon supported catalysts, directs toward wider use of green supporting material, BNC, for deposition of metallic nanoparticles, and its application in electrocatalysis. Findings presented in this study are very encouraging for the ongoing researches in the area of metallic particles-BNC catalytic systems.

Acknowledgements

This work was financially supported by the Ministry of Education, Science and Technological Development of the Republic of Serbia (contract No 451-03-68/2022-14/200026) and by the Science Fund of the Republic of Serbia under the grant No 7739802. Jasmina Nikodinovic-Runic

and Sanja Jeremic acknowledge support from the European Union's Horizon 2020 research and innovation programme under grant agreement No 870292 (BioICEP).

Conflicts of Interest: The authors declare no conflict of interest.

REFERENCES

[1] A. S. Aricò, S. Srinivasan, V. Antonucci, DMFCs: From Fundamental Aspects to Technology Development, Fuel Cells 1 (2001) 133-161. https://doi.org/10.1002/1615-6854(200107)1:2.

[2] H. Liu, C. Song, L. Zhang, J. Zhang, H. Wang, D. P. Wilkinson, A review of anode catalysis in the direct methanol fuel cell, J. Power Sources 155 (2006) 95-110. https://doi.org/10.1016/j.jpowsour.2006.01.030.

[3] G. Garcia, V. Baglio, A. Stassi, E. Pastor, V. Antonucci, A. S. Aricò, Investigation of Pt–Ru nanoparticle catalysts for low temperature methanol electro-oxidation, J. Solid State Electr. 11 (2007) 1229-1238. 10.1007/s10008-007-0274-8.

[4] J. Zeng, J. Yang, J. Y. Lee, W. Zhou, Preparation of Carbon-Supported Core−Shell Au−Pt Nanoparticles for Methanol Oxidation Reaction: The Promotional Effect of the Au Core, J. Phys. Chem. B 110 (2006) 24606-24611. 10.1021/jp0640979.

[5] P. Wang, Y. Wen, S. Yin, N. Wang, P. K. Shen, PtRh alloys on hybrid TiO2 – Carbon support as high efficiency catalysts for ethanol oxidation, Int. J. Hydrogen Energ. 42 (2017) 24689-24696. https://doi.org/10.1016/j.ijhydene.2017.04.302.

[6] A. K. Shukla, A. S. Aricò, K. M. El-Khatib, H. Kim, P. L. Antonucci, V. Antonucci, An X-ray photoelectron spectroscopic study on the effect of Ru and Sn additions to platinised carbons, Appl. Surf. Sci. 137 (1999) 20-29. https://doi.org/10.1016/S0169-4332(98)00483-8.

[7] V. M. Jovanović, S. Terzić, A. V. Tripković, K. D. Popović, J. D. Lović, The effect of electrochemically treated glassy carbon on the activity of supported Pt catalyst in methanol oxidation, Electrochem. Commun. 6 (2004) 1254-1258. https://doi.org/10.1016/j.elecom.2004.10.001.

[8] D. Mirabile Gattia, M. V. Antisari, L. Giorgi, R. Marazzi, E. Piscopiello, A. Montone, S. Bellitto, S. Licoccia, E. Traversa, Study of different nanostructured carbon supports for fuel cell catalysts, J. Power Sources 194 (2009) 243-251. https://doi.org/10.1016/j.jpowsour.2009.04.058.

[9] X. Mu, Z. Xu, Y. Xie, H. Mi, J. Ma, Pt nanoparticles supported on Co embedded coal-based carbon nanofiber for enhanced electrocatalytic activity towards methanol electro-oxidation, J. Alloy. Compd. 711 (2017) 374-380. https://doi.org/10.1016/j.jallcom.2017.04.008.

[10] L. Dong, R. R. S. Gari, Z. Li, M. M. Craig, S. Hou, Graphene-supported platinum and platinum–ruthenium nanoparticles with high electrocatalytic activity for methanol and ethanol oxidation, Carbon 48 (2010) 781-787. https://doi.org/10.1016/j.carbon.2009.10.027.

[11] X. Mu, Z. Xu, Y. Ma, Y. Xie, H. Mi, J. Ma, Graphene-carbon nanofiber hybrid supported Pt nanoparticles with enhanced catalytic performance for methanol oxidation

and oxygen reduction, Electrochim. Acta 253 (2017) 171-177. https://doi.org/10.1016/j.electacta.2017.09.029.

[12] X. Wu, C. Lu, Z. Zhou, G. Yuan, R. Xiong, X. Zhang, Green synthesis and formation mechanism of cellulose nanocrystal-supported gold nanoparticles with enhanced catalytic performance, Environ. Sci.-Nano 1 (2014) 71-79. 10.1039/C3EN00066D.

[13] J. C. Courtenay, R. I. Sharma, J. L. Scott, Recent Advances in Modified Cellulose for Tissue Culture Applications, Molecules 23 (2018) 654. 10.3390/molecules23030654.

[14] A. A. Oun, J.-W. Rhim, Isolation of cellulose nanocrystals from grain straws and their use for the preparation of carboxymethyl cellulose-based nanocomposite films, Carbohyd. Polym. 150 (2016) 187-200. https://doi.org/10.1016/j.carbpol.2016.05.020.

[15] K. L. Pickering, M. G. A. Efendy, T. M. Le, A review of recent developments in natural fibre composites and their mechanical performance, Compos. Part A-Appl. S. 83 (2016) 98-112. https://doi.org/10.1016/j.compositesa.2015.08.038.

[16] S. Azizi, M. B. Ahmad, M. Z. Hussein, N. A. Ibrahim, Synthesis, Antibacterial and Thermal Studies of Cellulose Nanocrystal Stabilized ZnO-Ag Heterostructure Nanoparticles, Molecules 18 (2013) 6269-6280. 10.3390/molecules18066269.

[17] M. Jonoobi, R. Oladi, Y. Davoudpour, K. Oksman, A. Dufresne, Y. Hamzeh, R. Davoodi, Different preparation methods and properties of nanostructured cellulose from various natural resources and residues: a review, Cellulose 22 (2015) 935-969. 10.1007/s10570-015-0551-0.

[18] X. Chen, F. Yuan, H. Zhang, Y. Huang, J. Yang, D. Sun, Recent approaches and future prospects of bacterial cellulose-based electroconductive materials, J. Mater. Sci. 51 (2016) 5573-5588. 10.1007/s10853-016-9899-2.

[19] F. Huang, W. Liu, P. Li, J. Ning, Q. Wei, Electrochemical Properties of LLTO/Fluoropolymer-Shell Cellulose-Core Fibrous Membrane for Separator of High Performance Lithium-Ion Battery, Materials 9 (2016) 75.

[20] C. Huang, H. Ji, B. Guo, L. Luo, W. Xu, J. Li, J. Xu, Composite nanofiber membranes of bacterial cellulose/halloysite nanotubes as lithium ion battery separators, Cellulose 26 (2019) 6669-6681. 10.1007/s10570-019-02558-y.

[21] S. Salimi, R. Sotudeh-Gharebagh, R. Zarghami, S. Y. Chan, K. H. Yuen, Production of Nanocellulose and Its Applications in Drug Delivery: A Critical Review, ACS Sustain. Chem. Eng. 7 (2019) 15800-15827. 10.1021/acssuschemeng.9b02744.

[22] N. F. Vasconcelos, J. P. A. Feitosa, F. M. P. da Gama, J. P. S. Morais, F. K. Andrade, M. d. S. M. de Souza Filho, M. d. F. Rosa, Bacterial cellulose nanocrystals produced under different hydrolysis conditions: Properties and morphological features, Carbohyd. Polym. 155 (2017) 425-431. https://doi.org/10.1016/j.carbpol.2016.08.090.

[23] C. Rovera, M. Ghaani, N. Santo, S. Trabattoni, R. T. Olsson, D. Romano, S. Farris, Enzymatic Hydrolysis in the Green Production of Bacterial Cellulose Nanocrystals, ACS Sustain. Chem. Eng. 6 (2018) 7725-7734. 10.1021/acssuschemeng.8b00600.

[24] S. Simić, S. Jeremic, L. Djokic, N. Božić, Z. Vujčić, N. Lončar, R. Senthamaraikannan, R. Babu, I. M. Opsenica, J. Nikodinovic-Runic, Development of an efficient biocatalytic system based on bacterial laccase for the oxidation of selected 1,4-dihydropyridines, Enzyme Microb. Tech. 132 (2020) 109411. https://doi.org/10.1016/j.enzmictec.2019.109411.

[25] K. E. Shopsowitz, H. Qi, W. Y. Hamad, M. J. MacLachlan, Free-standing mesoporous silica films with tunable chiral nematic structures, Nature 468 (2010) 422-425. 10.1038/nature09540.

[26] S. Jeremic, L. Djokic, V. Ajdačić, N. Božinović, V. Pavlovic, D. D. Manojlović, R. Babu, R. Senthamaraikannan, O. Rojas, I. Opsenica, J. Nikodinovic-Runic, Production of bacterial nanocellulose (BNC) and its application as a solid support in transition metal catalysed cross-coupling reactions, Int. J. Biol. Macromol. 129 (2019) 351-360. https://doi.org/10.1016/j.ijbiomac.2019.01.154.

[27] A. A. Oun, J.-W. Rhim, Characterization of carboxymethyl cellulose-based nanocomposite films reinforced with oxidized nanocellulose isolated using ammonium persulfate method, Carbohyd. Polym. 174 (2017) 484-492. https://doi.org/10.1016/j.carbpol.2017.06.121.

[28] N. Drogat, R. Granet, V. Sol, A. Memmi, N. Saad, C. Klein Koerkamp, P. Bressollier, P. Krausz, Antimicrobial silver nanoparticles generated on cellulose nanocrystals, J. Nanopart. Res. 13 (2011) 1557-1562. 10.1007/s11051-010-9995-1.

[29] A. Cañas-Gutiérrez, E. Martinez-Correa, D. Suárez-Avendaño, D. Arboleda-Toro, C. Castro-Herazo, Influence of bacterial nanocellulose surface modification on calcium phosphates precipitation for bone tissue engineering, Cellulose 27 (2020) 10747-10763. 10.1007/s10570-020-03470-6.

[30] H. Luo, G. Xiong, D. Hu, K. Ren, F. Yao, Y. Zhu, C. Gao, Wan, Characterization of TEMPO-oxidized bacterial cellulose scaffolds for tissue engineering applications, Mater. Chem. Phys. 143 (2013) 373-379. https://doi.org/10.1016/j.matchemphys.2013.09.012.

[31] C. Huang, H. Ji, Y. Yang, B. Gu, L. Luo, Z. Meng, L. Fan, J. Xu, TEMPO-oxidized bacterial cellulose nanofiber membranes as high-performance separators for lithium-ion batteries, Carbohyd. Polym. 230 (2020) 115570. https://doi.org/10.1016/j.carbpol.2019.115570.

[32] Y. Chen, S. Chen, B. Wang, L. Yao, H. Wang, TEMPO-oxidized bacterial cellulose nanofibers-supported gold nanoparticles with superior catalytic properties, Carbohyd. Polym. 160 (2017) 34-42. https://doi.org/10.1016/j.carbpol.2016.12.020.

[33] F. Peng, J. Xu, X. Zeng, G. Feng, H. Bao, Metal-Decorated Pickering Emulsion for Continuous Flow Catalysis, Part. Part. Syst. Char. 37 (2020) 1900382. https://doi.org/10.1002/ppsc.201900382.

[34] P. Zhou, H. Wang, J. Yang, J. Tang, D. Sun, W. Tang, Bio-supported palladium nanoparticles as a phosphine-free catalyst for the Suzuki reaction in water, RSC Advances 2 (2012) 1759-1761. http://doi.org/10.1039/C2RA01015A.

[35] C. Zhang, M. Zhou, S. Liu, B. Wang, Z. Mao, H. Xu, Y. Zhong, L. Zhang, B. Xu, X. Sui, Copper-loaded nanocellulose sponge as a sustainable catalyst for regioselective hydroboration of alkynes, Carbohyd. Polym. 191 (2018) 17-24. http://doi.org/10.1016/j.carbpol.2018.03.002.

[36] Y. Xu, K. Zhang, S. Chen, X. Zhang, Y. Chen, D. Li, F. Xu, Two-dimensional lamellar MXene/three-dimensional network bacterial nanocellulose nanofiber composite Janus membranes as nanofluidic osmotic power generators, Electrochim. Acta 412 (2022) 140162. https://doi.org/10.1016/j.electacta.2022.140162.

[37] J. Yang, D. Sun, J. Li, X. Yang, J. Yu, Q. Hao, W. Liu, J. Liu, Z. Zou, J. Gu, In situ deposition of platinum nanoparticles on bacterial cellulose membranes and evaluation of

PEM fuel cell performance, Electrochim. Acta 54 (2009) 6300-6305. https://doi.org/10.1016/j.electacta.2009.05.073.

[38] Y. Huang, T. Wang, M. Ji, J. Yang, C. Zhu, D. Sun, Simple preparation of carbonized bacterial cellulose–Pt composite as a high performance electrocatalyst for direct methanol fuel cells (DMFC), Mater. Lett. 128 (2014) 93-96. https://doi.org/10.1016/j.matlet.2014.04.128.

[39] T.-J. Wang, H. Huang, X.-R. Wu, H.-C. Yao, F.-M. Li, P. Chen, P.-J. Jin, Z.-W. Deng, Y. Chen, Self-template synthesis of defect-rich NiO nanotubes as efficient electrocatalysts for methanol oxidation reaction, Nanoscale 11 (2019) 19783-19790. http://doi.org/10.1039/C9NR06304H.

[40] H. Wang, K. Zhang, J. Qiu, J. Wu, J. Shao, H. Wang, Y. Zhang, J. Han, Y. Zhang, L. Yan, Ternary PtFeCo alloys on graphene with high electrocatalytic activities for methanol oxidation, Nanoscale 12 (2020) 9824-9832. http://doi.org/10.1039/D0NR00757A.

[41] P. E. Lokhande, P. P. Singh, D.-V. N. Vo, D. Kumar, K. Balasubramanian, A. Mubayi, A. Srivastava, A. Sharma, Bacterial nanocellulose: Green polymer materials for high performance energy storage applications, J. Environ. Chem. Eng. 10 (2022) 108176. https://doi.org/10.1016/j.jece.2022.108176.

[42] J. M. Doña Rodríguez, J. A. Herrera Melián, J. Pérez Peña, Determination of the Real Surface Area of Pt Electrodes by Hydrogen Adsorption Using Cyclic Voltammetry, J. Chem. Ed. 77 (2000) 1195. 10.1021/ed077p1195.

[43] E. Lam, A. C. W. Leung, Y. Liu, F. Majid, S. Hrapovic, K. B. Male, J. H. T. Luong, Green Strategy Guided by Raman Spectroscopy for the Synthesis of Ammonium Carboxylated Nanocrystalline Cellulose and the Recovery of Byproducts, ACS Sustain. Chem. Eng. 1 (2013) 278-283. http://doi.org/10.1021/sc3001367.

[44] A. A. Oun, J.-W. Rhim, Characterization of nanocelluloses isolated from Ushar (Calotropis procera) seed fiber: Effect of isolation method, Mater. Lett. 168 (2016) 146-150. https://doi.org/10.1016/j.matlet.2016.01.052.

[45] M. Park, B.-H. Kim, S. Kim, D.-S. Han, G. Kim, K.-R. Lee, Improved binding between copper and carbon nanotubes in a composite using oxygen-containing functional groups, Carbon 49 (2011) 811-818. https://doi.org/10.1016/j.carbon.2010.10.019.

[46] S. H. Hassan, N. S. Velayutham, Y. W. Chen, H. V. Lee, TEMPO-oxidized nanocellulose films derived from coconut residues: Physicochemical, mechanical and electrical properties, Int. J. Biol. Macromol. 180 (2021) 392-402. https://doi.org/10.1016/j.ijbiomac.2021.03.066.

[47] P. Lu, Y.-L. Hsieh, Preparation and properties of cellulose nanocrystals: Rods, spheres, and network, Carbohyd. Polym. 82 (2010) 329-336. https://doi.org/10.1016/j.carbpol.2010.04.073.

[48] F. Jiang, Y.-L. Hsieh, Chemically and mechanically isolated nanocellulose and their self-assembled structures, Carbohydrate Polymers 95 (2013) 32-40. https://doi.org/10.1016/j.carbpol.2013.02.022.

[49] A. Isogai, T. Saito , H. Fukuzumi, TEMPO-oxidized cellulose nanofibers, Nanoscale 3 (2011) 71-85. http://doi.org/10.1039/C0NR00583E.

[50] Y. Ding, L. Zhang, Q. Gu, I. Spanos, N. Pfänder, K. H. Wu, R. Schlögl, S. Heumann, Tuning of Reciprocal Carbon-Electrode Properties for an Optimized Hydrogen Evolution, Chem. Sustain. Chem. 14 (2021) 2547-2553. https://doi.org/10.1002/cssc.202100654.

[51] S. Li, Z. Jiang, A. Liu, J. Lu, J. Du, Y. Tao, Y. Cheng, H. Wang, A porous carbon based on the surface and structural regulation of wasted lignin for long-cycle lithium-ion battery, Int. J. Biol. Macromol. 222 (2022) 1414-1422. https://doi.org/10.1016/j.ijbiomac.2022.09.269.

[52] M. A. Henrique, W. P. Flauzino Neto, H. A. Silvério, D. F. Martins, L. V. A. Gurgel, H. d. S. Barud, L. C. d. Morais, D. Pasquini, Kinetic study of the thermal decomposition of cellulose nanocrystals with different polymorphs, cellulose I and II, extracted from different sources and using different types of acids, Ind. Crop. Prod. 76 (2015) 128-140. https://doi.org/10.1016/j.indcrop.2015.06.048.

[53] A. D. French, Idealized powder diffraction patterns for cellulose polymorphs, Cellulose 21 (2014) 885-896. http://doi.org/10.1007/s10570-013-0030-4.

[54] K. Zhang, H. Wang, J. Qiu, J. Wu, H. Wang, J. Shao, Y. Deng, L. Yan, Multi-dimensional Pt/Ni(OH)2/nitrogen-doped graphene nanocomposites with low platinum content for methanol oxidation reaction with highly catalytic performance, Chem. Eng. J. 421 (2021) 127786. https://doi.org/10.1016/j.cej.2020.127786.

[55] M. N. Krstajić Pajić, S. I. Stevanović, V. V. Radmilović, A. Gavrilović-Wohlmuther, V. R. Radmilović, S. L. Gojković, V. M. Jovanović, Shape evolution of carbon supported Pt nanoparticles: From synthesis to application, Appl. Catal. B-Environ. 196 (2016) 174-184. https://doi.org/10.1016/j.apcatb.2016.05.033.

[56] A. Esfandiari, M. Kazemeini , D. Bastani, Synthesis, characterization and performance determination of an Ag@Pt/C electrocatalyst for the ORR in a PEM fuel cell, Int. J. Hydrogen Energ. 41 (2016) 20720-20730. https://doi.org/10.1016/j.ijhydene.2016.09.097.

[57] B. Ruiz-Camacho, A. Medina-Ramírez, R. Fuentes-Ramírez, R. Navarro, C. Martínez Goméz, A. Pérez-Larios, Pt and Pt–Ag nanoparticles supported on carbon nanotubes (CNT) for oxygen reduction reaction in alkaline medium, Int. J. Hydrogen Energ. 47 (2022) 30147-30159. https://doi.org/10.1016/j.ijhydene.2022.03.190.

[58] L.-S. Johansson, J. M. Campbell, Reproducible XPS on biopolymers: cellulose studies, Surf. Interface Anal. 36 (2004) 1018-1022. https://doi.org/10.1002/sia.1827.

[59] D. Pawcenis, E. Twardowska, M. Leśniak, R. J. Jędrzejczyk, M. Sitarz, J. Profic-Paczkowska, TEMPO-oxidized cellulose for in situ synthesis of Pt nanoparticles. Study of catalytic and antimicrobial properties, Int. J. Biol. Macromol. 213 (2022) 738-750. https://doi.org/10.1016/j.ijbiomac.2022.06.020.

[60] T.-J. Wang, H.-Y. Sun, Q. Xue, M.-J. Zhong, F.-M. Li, X. Tian, P. Chen, S.-B. Yin, Y. Chen, Holey platinum nanotubes for ethanol electrochemical reforming in aqueous solution, Sci. Bull. 66 (2021) 2079-2089. https://doi.org/10.1016/j.scib.2021.05.027.

[61] X. Tian, J. Luo, H. Nan, H. Zou, R. Chen, T. Shu, X. Li, Y. Li, H. Song, S. Liao, R. R. Adzic, Transition Metal Nitride Coated with Atomic Layers of Pt as a Low-Cost, Highly Stable Electrocatalyst for the Oxygen Reduction Reaction, J. Am. Chem. Soc. 138 (2016) http://doi.org/1575-1583. 10.1021/jacs.5b11364.

[62] H. Kim, G.-h. Kwon, S. O. Han, A. Robertson, Platinum Encapsulated within a Bacterial Nanocellulosic–Graphene Nanosandwich as a Durable Thin-Film Fuel Cell Catalyst, ACS Appl. Energ. Mater. 4 (2021) 1286-1293. http://doi.org/10.1021/acsaem.0c02533.

[63] D. Tripković, S. Stevanović, A. Gavrilović, J. Rogan, U. Lačnjevac, T. Kravić, V. M. Jovanović, The Role of SnO2 on Electrocatalytic Activity of PtSn Catalysts, Electrocatalysis 9 (2018) 76-85. 10.1007/s12678-017-0424-4.

[64] S. Stevanović, D. Tripković, V. Tripković, D. Minić, A. Gavrilović, A. Tripković, V. M. Jovanović, Insight into the Effect of Sn on CO and Formic Acid Oxidation at PtSn Catalysts, J. Phys. Chem. C 118 (2014) 278-289. http://doi.org/10.1021/jp408207u.

[65] J. Solla-Gullón, P. Rodríguez, E. Herrero, A. Aldaz, J. M. Feliu, Surface characterization of platinum electrodes, Phys. Chem. Chem. Phys. 10 (2008) 1359-1373. http://doi.org/10.1039/B709809J.

[66] T. Iwasita, Electrocatalysis of methanol oxidation, Electrochim. Acta 47 (2002) 3663-3674. https://doi.org/10.1016/S0013-4686(02)00336-5.

[67] H. Tian, Y. Yu, Q. Wang, J. Li, P. Rao, R. Li, Y. Du, C. Jia, J. Luo, P. Deng, Y. Shen, X. Tian, Recent advances in two-dimensional Pt based electrocatalysts for methanol oxidation reaction, Int. J. Hydrogen Energ. 46 (2021) 31202-31215. https://doi.org/10.1016/j.ijhydene.2021.07.006.

[68] H. F. Beden B, C. Lamy, J. M. Leger, N. R. Tacconi, R. O. Lezna, A. J. Arvia, J. Electroanal. Chem. 261 (1989) 401-408.

[69] M. N. K. Pajić, S. I. Stevanović, V. V. Radmilović, J. P. Regan, V. R. Radmilović, S. L. Gojković, V. M. Jovanović, Pt/C nanocatalysts for methanol electrooxidation prepared by water-in-oil microemulsion method, J. Solid State Electr. 20 (2016) 3405-3414. http://doi.org/10.1007/s10008-016-3319-z.

[70] S. Stevanovic, A. Gavrilovic-Wohlmuther, J. Rogan, U. Lacnjevac, V. Jovanovic, Carbon Supported PtSn versus $PtSnO_2$ catalysts in methanol oxidation, Int. J. Electrochem. Sci. 16 (2021) 1-15. 10.20964/2021.02.55.

[71] K. Kinoshita, Particle Size Effects for Oxygen Reduction on Highly Dispersed Platinum in Acid Electrolytes, J. Electrochem. Soc. 137 (1990) 845-848. 10.1149/1.2086566.

[72] L. Zhang, D. Xia, Electrocatalytic activity of ordered intermetallic PtSb for methanol electro-oxidation, Appl. Surf. Sci. 252 (2006) 2191-2195. https://doi.org/10.1016/j.apsusc.2005.03.221.

[73] Y.-W. Lee, A. R. Ko, S.-B. Han, H.-S. Kim, K.-W. Park, Synthesis of octahedral Pt–Pd alloy nanoparticles for improved catalytic activity and stability in methanol electrooxidation, Phys. Chem. Chem. Phys. 13 (2011) 5569-5572. http://doi.org/10.1039/C0CP02167A.

[74] A. Tripkovic, K. Dj. Popovic, J. D. Lovic, Methanol oxidation at platinum electrodes in acid solution: comparison between model and real catalysts, J. Serb. Chem. Soc. 71 (2006) 1333-1343.

[75] X. Zhao, J. Zhu, L. Liang, C. Li, C. Liu, J. Liao, W. Xing, Biomass-derived N-doped carbon and its application in electrocatalysis, Appl. Catal. B-Environ. 154–155 (2014) 177–18. http://dx.doi.org/10.1016/j.apcatb.2014.02.027

[76] F. Yuan,Y. Huang, M. Fan, C. Chen, J. Qian, Q. Hao, J. Yang, D. Sun, N-Doped Carbon Nanofibrous Network Derived from Bacterial Cellulose for the Loading of Pt Nanoparticles for Methanol Oxidation Reaction, Chem. Eur. J. 24 (2018) 1844 – 1852. https://doi.org/10.1002/chem.201704266

Figure captions

Figure 1. Schematic illustration of synthetic procedure of Pt/BNC catalyst.

Figure 2. FTIR analysis of the raw BNC and Pt/BNC.

Figure 3. a) DSC thermograms of raw BNC and Pt/BNC catalyst, b) TGA curves and inserted DTGA curves of BNC, modified BNC, *m*-BNC, and Pt/BNC catalyst.

Figure 4. XRD difgractograms of BNC and Pt/BNC catalyst.

Figure 5. a) 2D images and section analysis of BNC (2 × 2 × 0.25 μm) and Pt/BNC (1 × 1 × 0.2 μm) and b) TEM images of raw BNC (magnification of 80k) and Pt/BNC catalyst (magnification of 100k).

Figure 6. XPS analysis: a) survey spectrum of Pt BNC catalyst, b) deconvoluted C 1s spectrum, c) deconvoluted O 1s spectrum, and d) deconvoluted Pt 4f spectrum.

Figure 7. a) Cyclic voltammogram of *as-prepared* Pt/BNC catalyst in 0.1 M H_2SO_4, v = 50 mV/s, b) cyclic voltammogram recorded in 0.5 M CH_3OH + 0.1 M H_2SO_4 at Pt/BNC catalyst, v = 50 mV/s, c) Long-term stability for the first and 100^{th} sweep (black line represents 1^{th} sweep and blue line is 100^{th} sweep) H_2SO_4/CH_3OH solution and d)chronoamperometric measurement for Pt/BNC catalyst in H_2SO_4/CH_3OH solution.

Figure 1

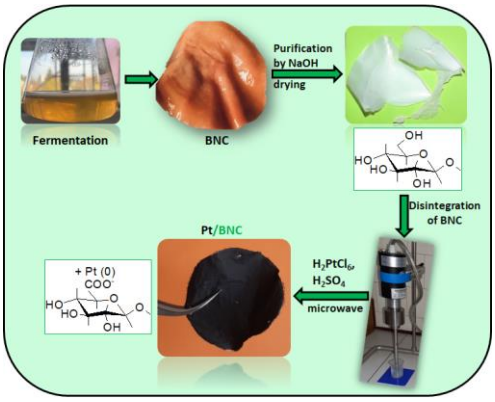

Figure 2

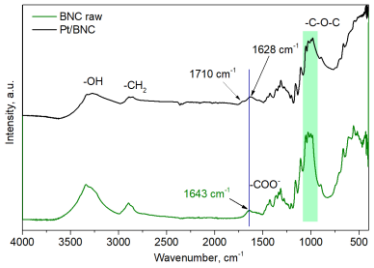

Figure 3

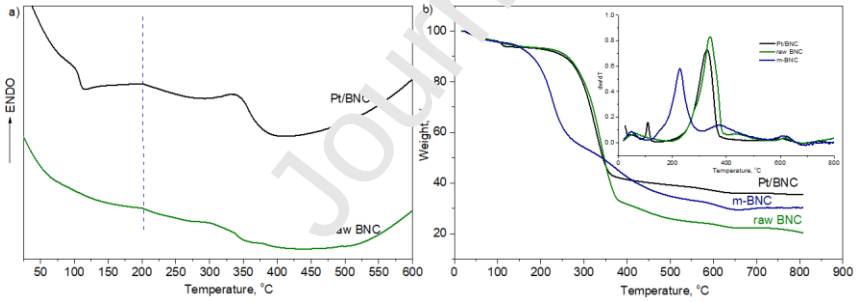

Figure 4

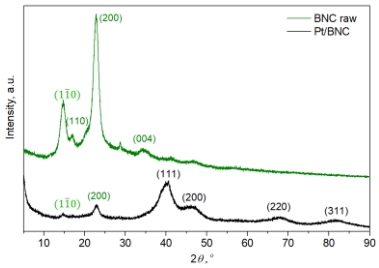

Figure 5

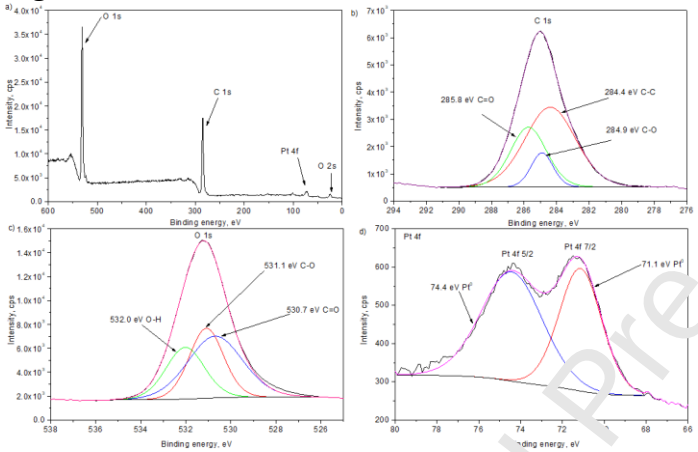

Figure 6

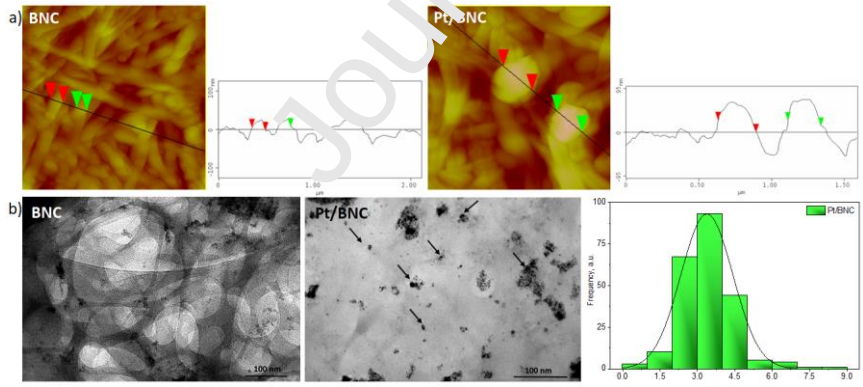

Figure 7

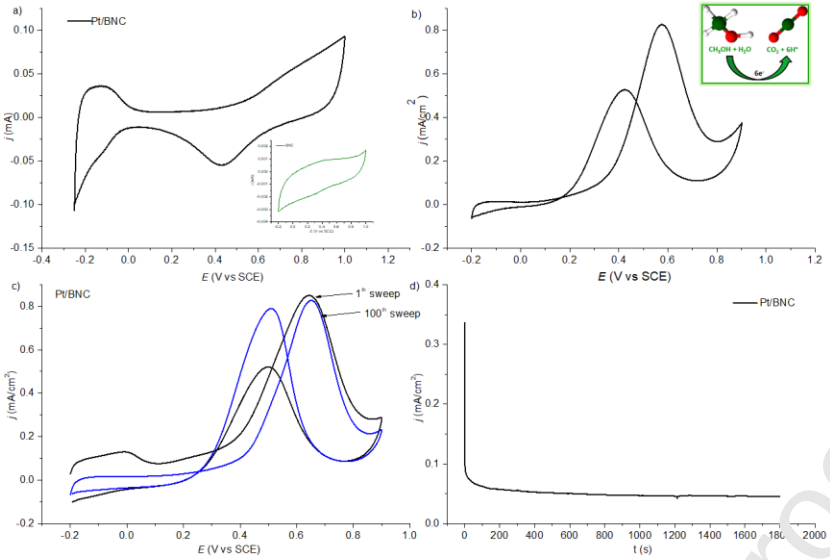

Authors statement

All authors have approved the final version of the manuscript. We confirm that this work is original and has not been published elsewhere nor is currently under consideration for publication elsewhere and will not be submitted for such a review while under review by the *International Journal of Biological Macromolecules.* The manuscript contains no libelous or other unlawful statements and does not contain any materials that violate any person or proprietary rights of any other person or entity.

Declaration of interests

☒The authors declare that they have no known competing financial interests or personal relationships that could have appeared to influence the work reported in this paper.

☐The authors declare the following financial interests/personal relationships which may be considered as potential competing interests:

Graphical abstract

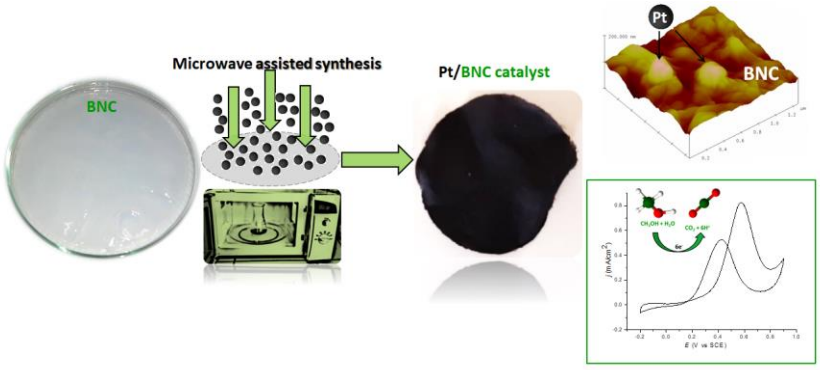

Highlights

- The new platinum supported bacterial nanocellulose catalyst (Pt/BNC) was successfully synthesized by microwave assisted method.
- The implementation of new catalyst was investigated for methanol oxidation reaction where desirable catalytic activity was achieved.
- Potential substitution of carbon based materials in the electrochemistry area as platinum nanoparticles support with the green one, bacterial nanocellulose.

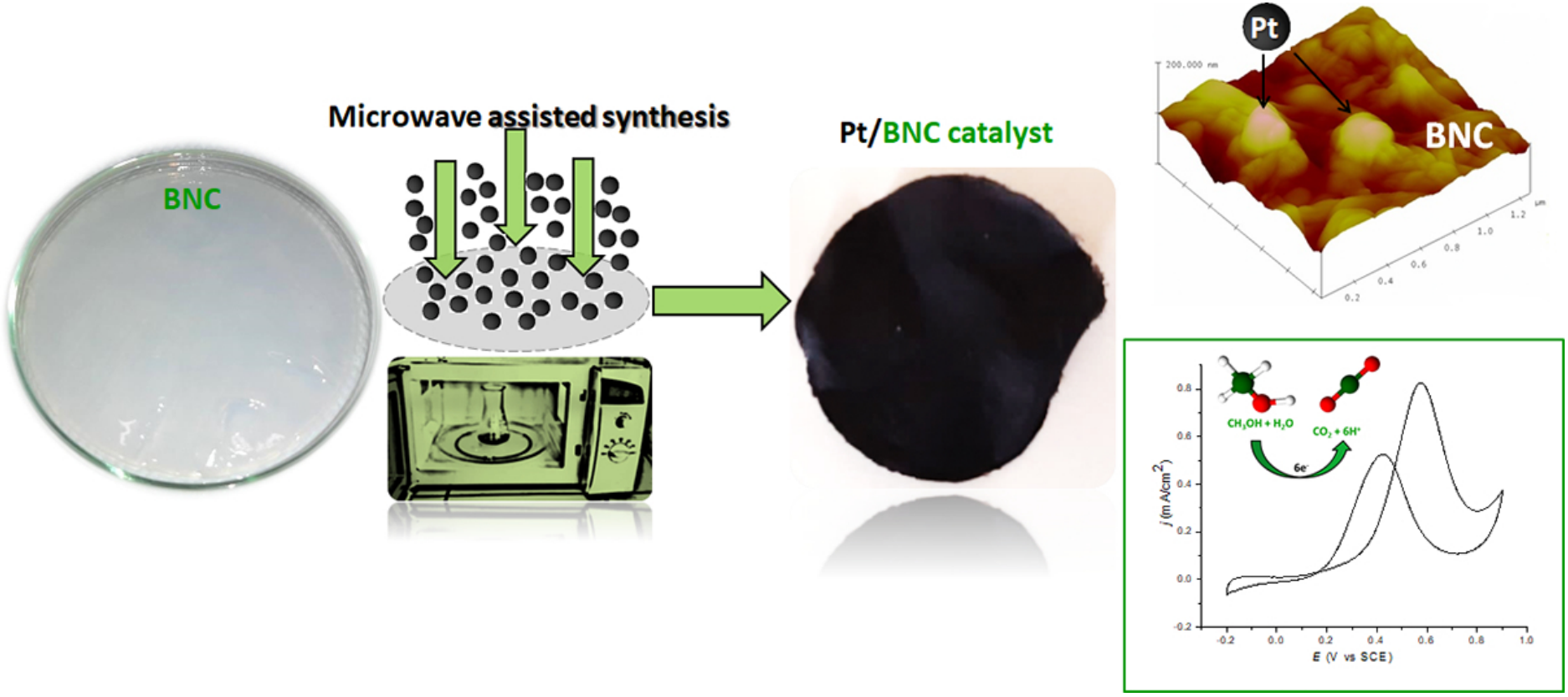

Graphics Abstract

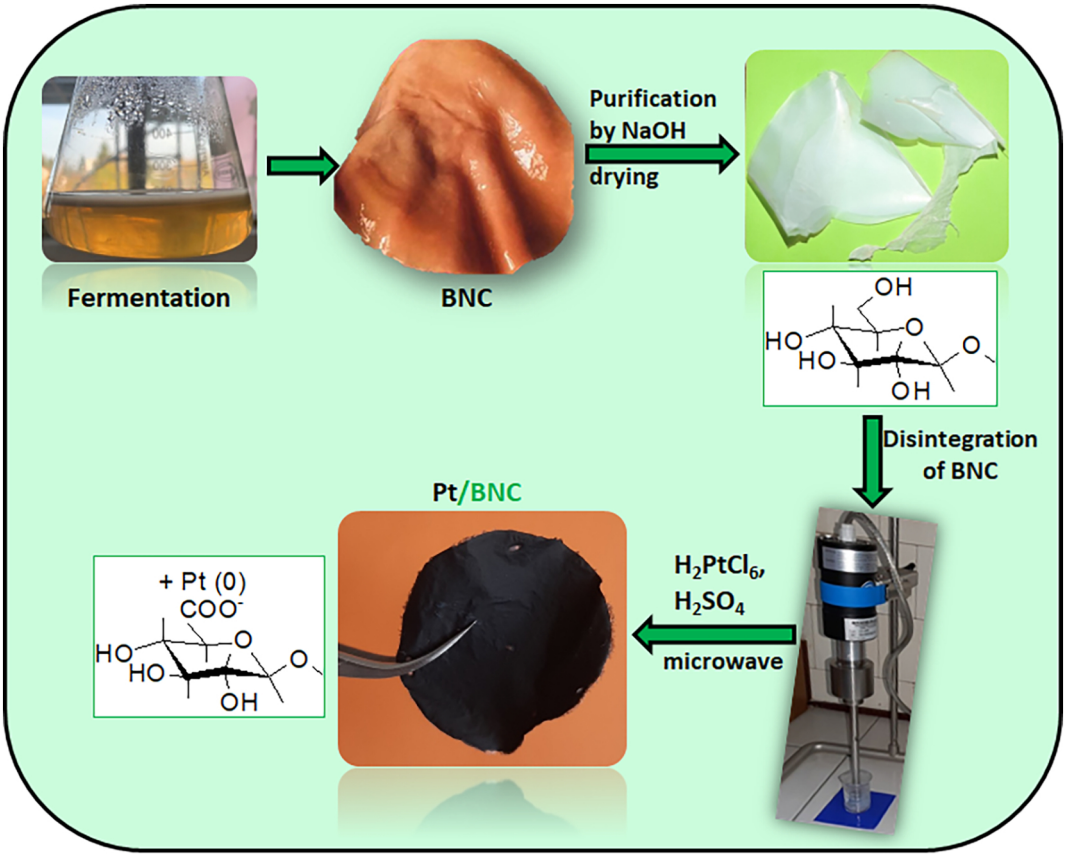
Fermentation
BNC
Purification
by NaOH
drying
Disintegration
of BNC
H_2PtCl_6,
H_2SO_4
microwave
Pt/BNC
+ Pt (0)

Figure 1

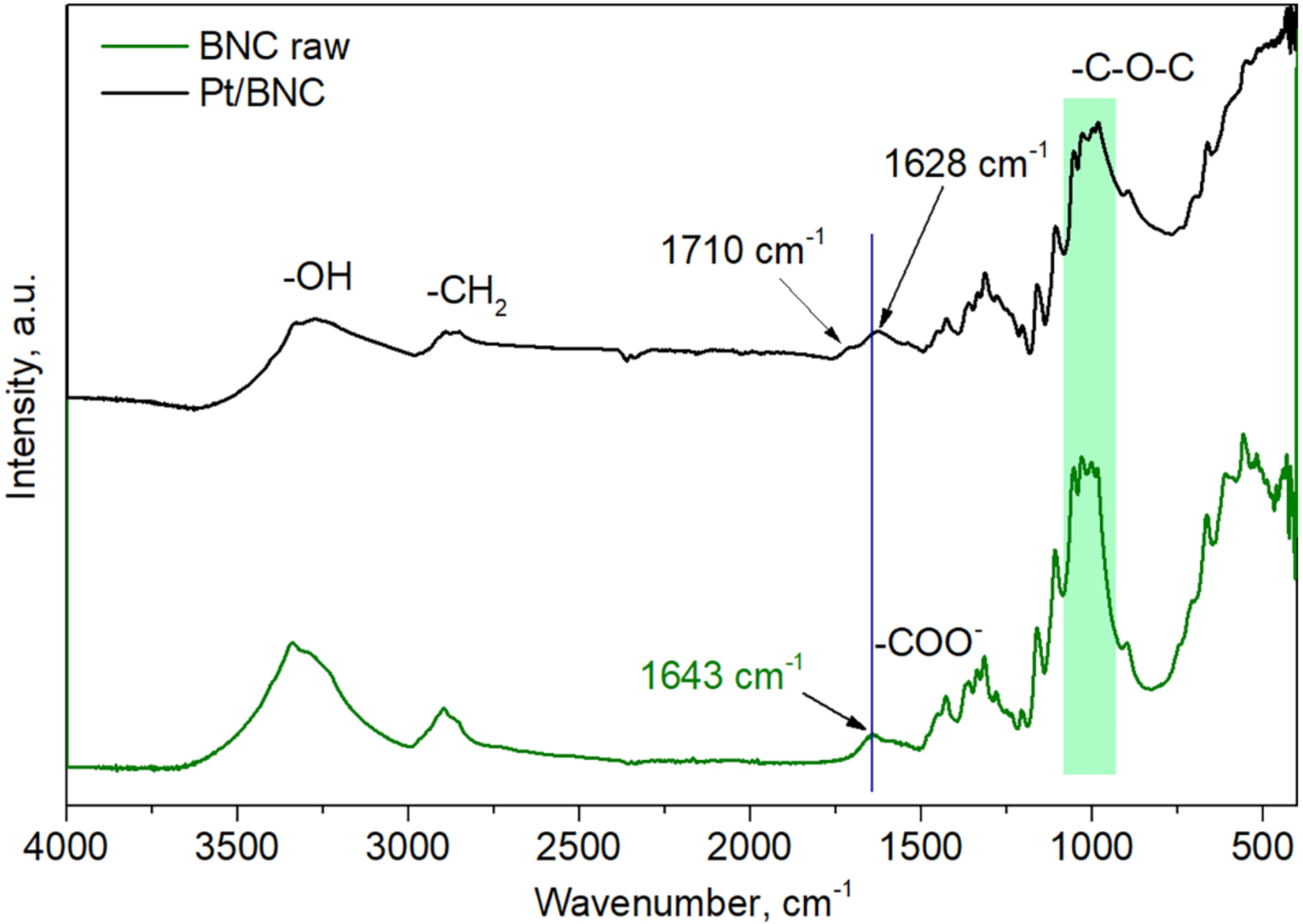
BNC raw
Pt/BNC
-C-O-C
1628 cm-1
1710 cm-1
-OH
-CH2
-COO-
1643 cm-1
Intensity, a.u.
4000
3500
3000
2500
2000
1500
1000
500
Wavenumber, cm-1

Figure 2

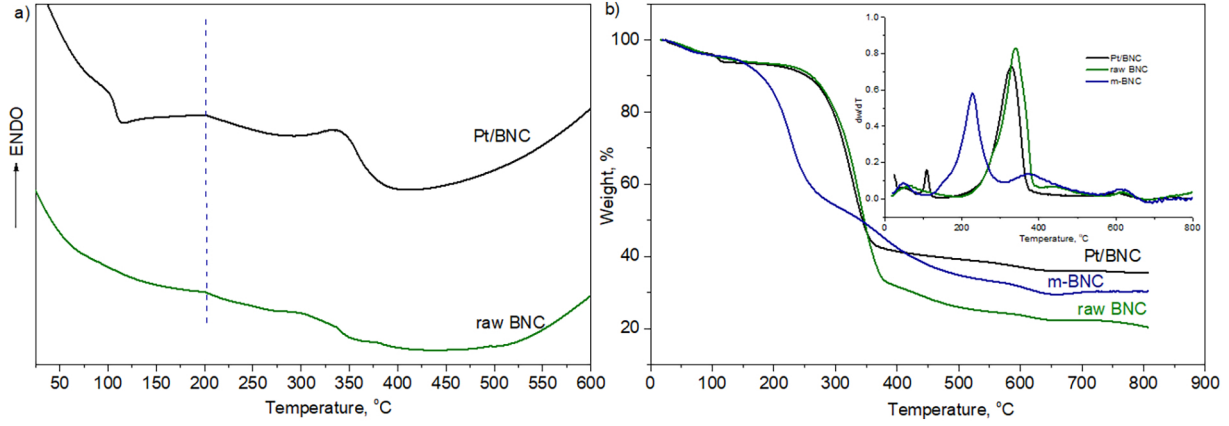
a)
ENDO
Pt/BNC
raw BNC
50 100 150 200 250 300 350 400 450 500 550 600
Temperature, °C
b)
Weight, %
100
80
60
40
20
0 100 200 300 400 500 600 700 800 900
Temperature, °C
Pt/BNC
m-BNC
raw BNC
dw/dT
1.0
0.8
0.6
0.4
0.2
0.0
0 200 400 600 800
Temperature, °C
Pt/BNC
raw BNC
m-BNC

Figure 3

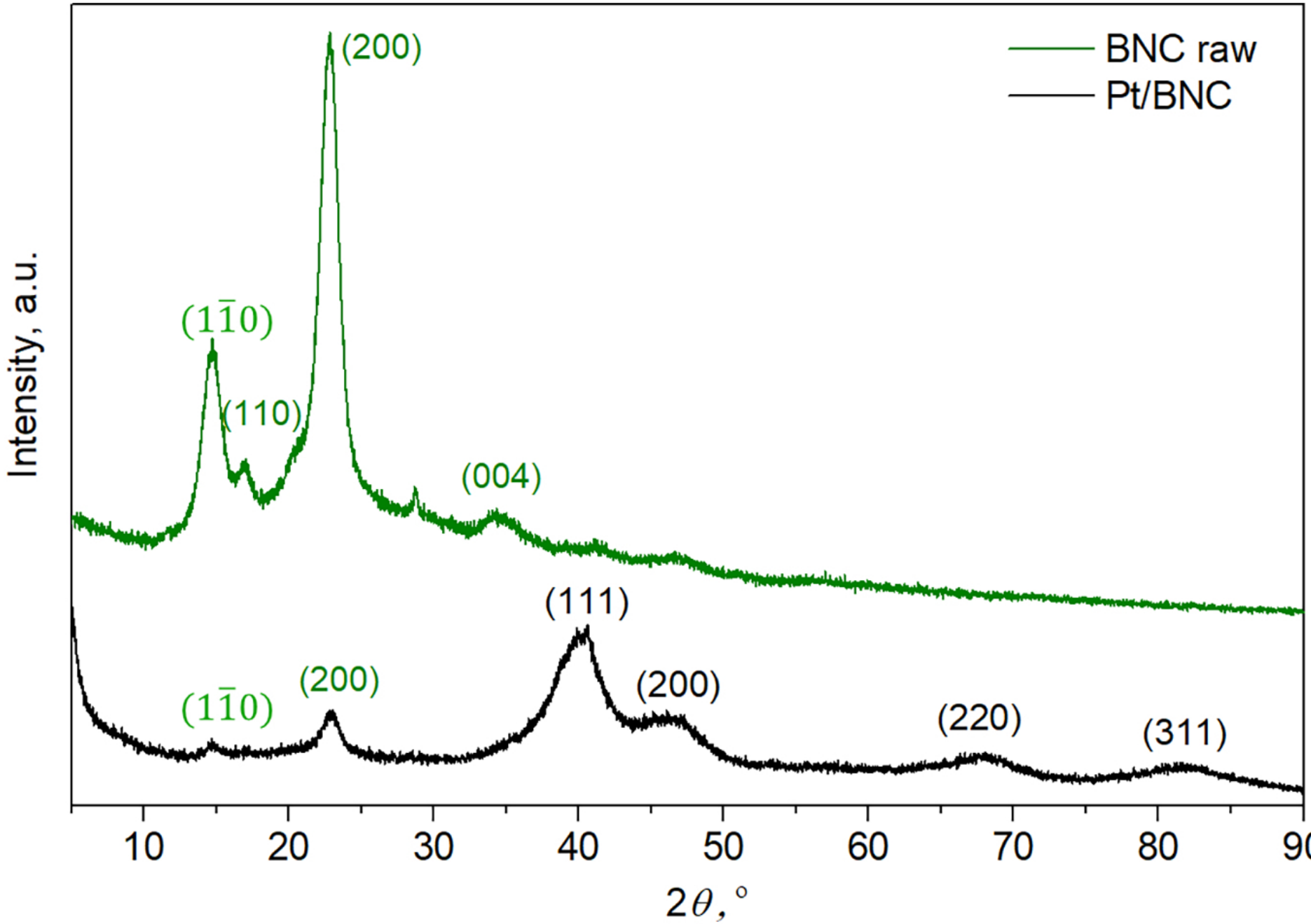
BNC raw
Pt/BNC
(200)
(1$\bar{1}$0)
(110)
(004)
(111)
(1$\bar{1}$0)
(200)
(200)
(220)
(311)
Intensity, a.u.
10
20
30
40
50
60
70
80
90
2θ,°

Figure 4

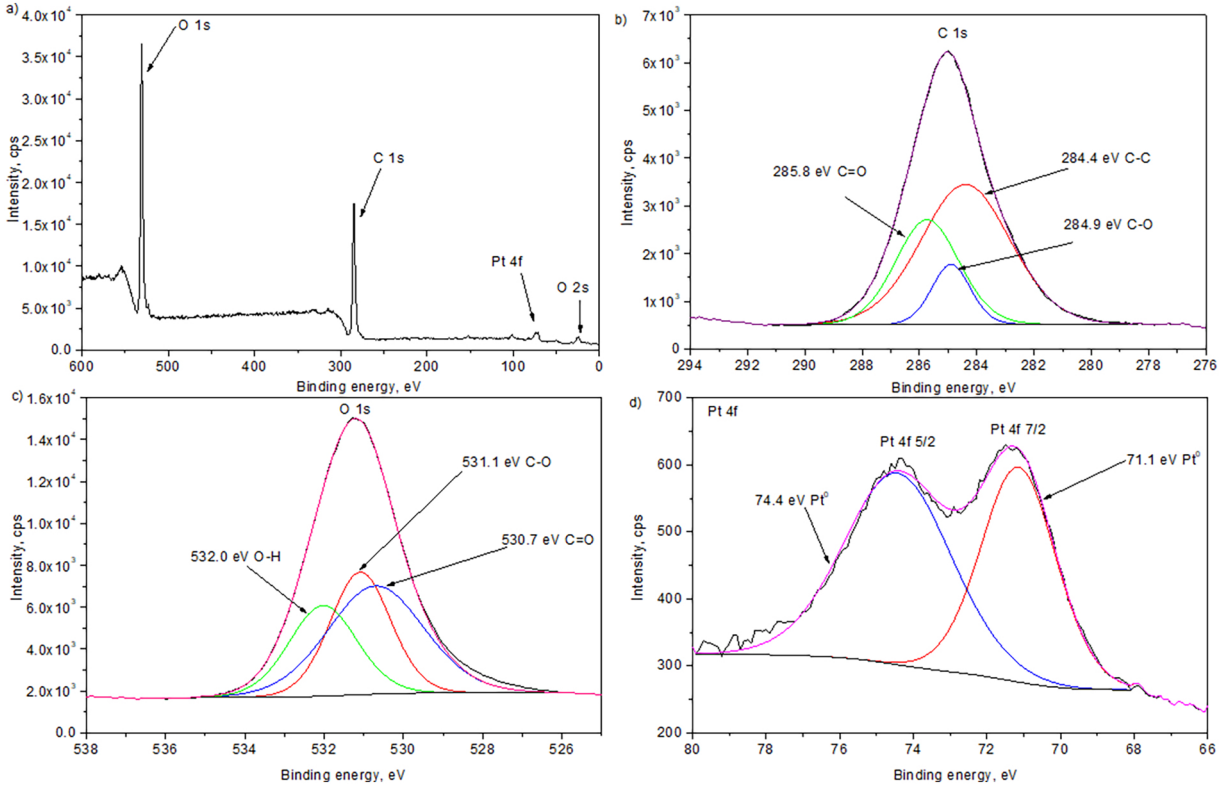
a)
O 1s
C 1s
Pt 4f
O 2s
Intensity, cps
Binding energy, eV
b)
C 1s
285.8 eV C=O
284.4 eV C-C
284.9 eV C-O
Intensity, cps
Binding energy, eV
c)
O 1s
531.1 eV C-O
532.0 eV O-H
530.7 eV C=O
Intensity, cps
Binding energy, eV
d)
Pt 4f
Pt 4f 5/2
Pt 4f 7/2
74.4 eV Pt°
71.1 eV Pt°
Intensity, cps
Binding energy, eV

Figure 5

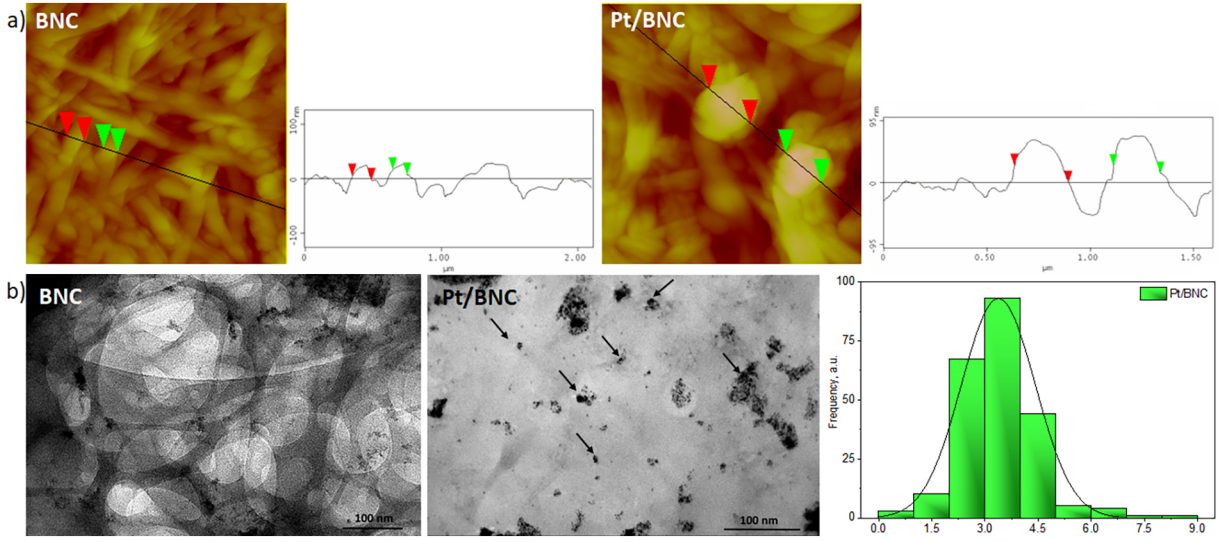
a)
BNC
100 nm
0
-100
0
1.00
2.00
μm
Pt/BNC
95 nm
0
-95
0
0.50
1.00
1.50
μm
b)
BNC
100 nm
Pt/BNC
100 nm
Pt/BNC
Frequency, a.u.
100
75
50
25
0
0.0
1.5
3.0
4.5
6.0
7.5
9.0

Figure 6

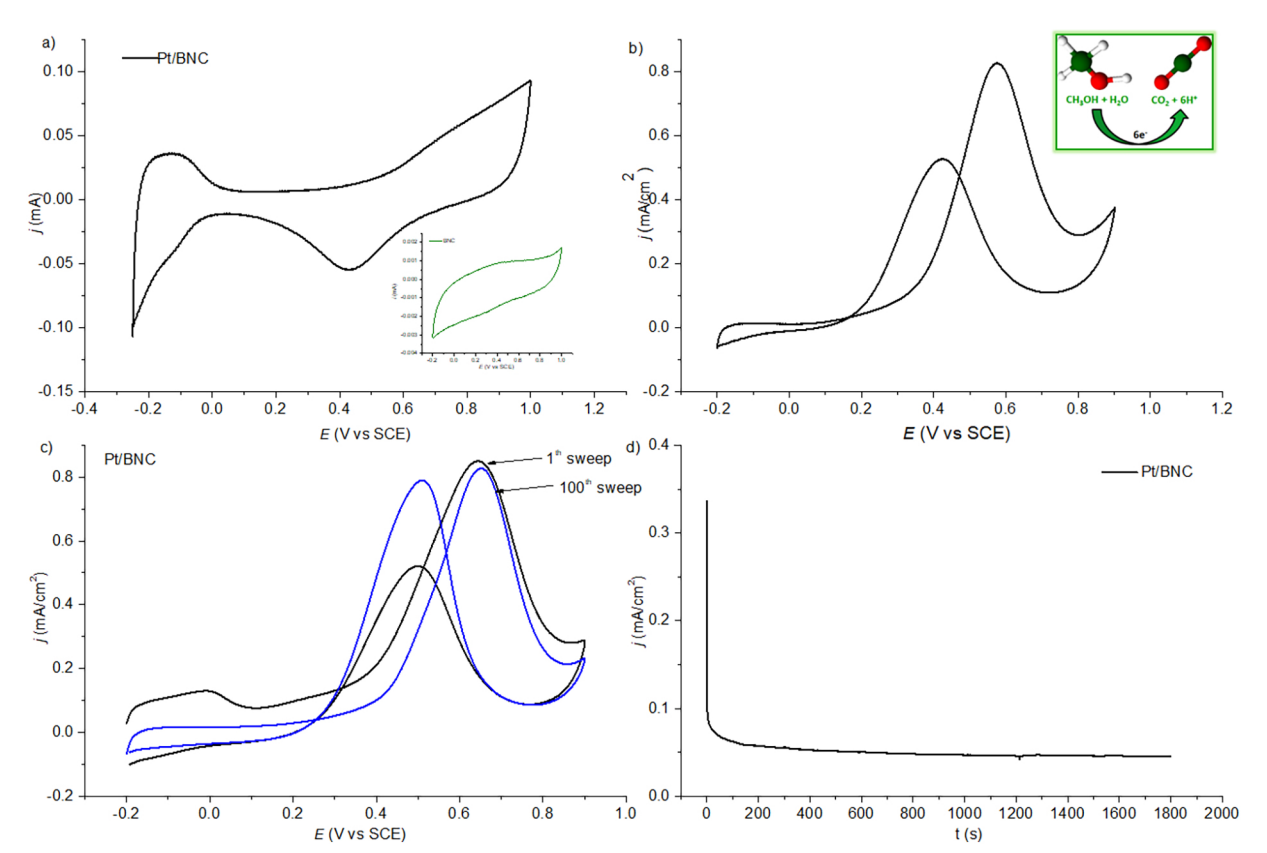
a)
Pt/BNC
j (mA)
E (V vs SCE)
b)
j (mA/cm2)
E (V vs SCE)
CH3OH + H2O
CO2 + 6H+
6e-
c)
Pt/BNC
1th sweep
100th sweep
j (mA/cm2)
E (V vs SCE)
d)
Pt/BNC
j (mA/cm2)
t (s)

Figure 7